GOSPODARKA SUROWCAMI MINERALNYMI – MINERAL RESOURCES MANAGEMENT

2025 Volume 41 Issue 4 Pages 153–173

DOI: 10.24425/gsm.2025.155884

SUFRIADIN SUFRIADIN[1], NAUFAL MUTAWALLY DAMRIADI[2], FRYAN FATLI[3], PURWANTO PURWANTO[4], RIZKI AMALIA[5], AKHIRUDDIN MADDU[6], AKANE ITO[7], AKMAL SAPUTNO[8]

# Beneficiation of a lateritic nickel ore from the Wolo Mine area, Southeast Sulawesi, Indonesia, through reductive roasting and magnetic separation

## Introduction

Nickel has played a crucial role and has numerous applications in the industrial sectors. Approximately 62% of nickel production is used for stainless steel manufacturing, while the rest is utilized for producing superalloys and non-ferrous alloys (Nickel Institute 2023).

✉ Corresponding Author: Sufriadin Sufriadin; e-mail: sufri.as@unhas.ac.id

[1] Department of Mining Engineering, Hasanuddin University, Indonesia; ORCID iD: 0000-0002-6103-3143; e-mail: sufri.as@unhas.ac.id

[2] Department of Mining Engineering, Hasanuddin University, Indonesia; e-mail: naufal.damriadi@gmail.com

[3] Department of Mining Engineering, Hasanuddin University, Indonesia; e-mail: fryanfatli13@gmail.com

[4] Department of Mining Engineering, Hasanuddin University, Indonesia; Scopus ID: 57112277800; e-mail: purwanto@unhas.ac.id

[5] Department of Mining Engineering, Hasanuddin University, Indonesia; e-mail: rizkiamalia543@yahoo.com

Nickel can be recovered either from sulfides or laterite ores. Lateritic nickel ore is formed by the chemical weathering process of ultramafic rocks in tropical or previously subtropical regions, often found on low-lying and flat land surfaces called peneplains (Butt and Cluzel 2013). The nickel laterite ores are generally classified into two types: saprolite, located in the lower profile, primarily contains hydro-silicates as Ni-bearing minerals such as serpentine and talc. It tends to have a high Ni and Mg content but is lower in Co and Fe. In contrast, limonite is situated in the upper profile, minerals, such as goethite and hematite. It is characterized by lower Ni but higher Co and Fe (Nurjaman et al. 2021). A steady increase in mine production from laterite ores has led to a decline in higher-grade Ni ore reserves in the last few years.

To maintain sustainable Ni production, it is anticipated that the utilization of lower-grade Ni laterite ores is inevitable. However, the low-cost physical beneficiation of Ni laterite ore is generally not practically employed directly because Ni is not present as discrete minerals but occurs as an intimate substitution for iron or magnesium in the main mineral structures (Fan et al. 2024). It is, therefore, necessary to seek efficient ways to treat Ni laterite ore before the smelting process.

Previous studies reported that reduction roasting of nickel laterite ore followed by magnetic separation to increase Ni grade or produce ferronickel concentrates in a solid state was feasible (Elliot et al. 2016; Chen et al. 2016; Elliot et al. 2017; Zappala et al. 2024). Studies conducted by Kim et al. (2010) suggested that the nickel grade of laterite ore could be upgraded from 1.50% up to 2.90% after the ore was calcined at 500°C and then separated by wet magnetic method. However, the recovery rates were low, only 48%.

The reduction roasting and magnetic separation method is critical to increasing the nickel content in nickel laterite ore, especially in low-grade laterite ore (Forster et al. 2016; Subagja et al. 2016). Although the reduction roasting and magnetic separation method can potentially improve the nickel content of laterite ore, however, many factors and parameters must be considered to achieve optimal results, such as roasting temperature, roasting time, ore-to-reductant ratio, and particle size. This study aimed to analyze the effects of particle size on Fe-Ni enrichment, compare the Ni recoveries between unroasted and roasted concentrates using a magnetic separator, and discuss the reduction and metallization process of Fe-Ni using corncob charcoal as a reductant.

[6] Department of Physics, Faculty of Science, IPB University, Indonesia; ORCID iD: 0000-0002-7477-0599; Scopus ID: 23477443900; e-mail: akhiruddin@apps.ipb.ac.id
[7] Department of Earth Resources Engineering, Kyushu University, Japan; ORCID iD: 0000-0001-6406-3156; Scopus ID: 57194237582; e-mail: aito@mine.kyushu-u.ac.jp
[8] Institute of Geological Science, Jagiellonian University, Krakow, Poland; Scopus ID: 58088034400; e-mail: akmalputno@gmail.com

# 1. Materials and methods

## 1.1. Materials

A nickel laterite ore sample used in this study was taken from a nickel laterite mine face owned by PT. CNI, a national mining company, located in the Wolo District of Kolaka Regency, Southeast Sulawesi, Indonesia (Figure 1). The sample was then air-dried, homogenized, and

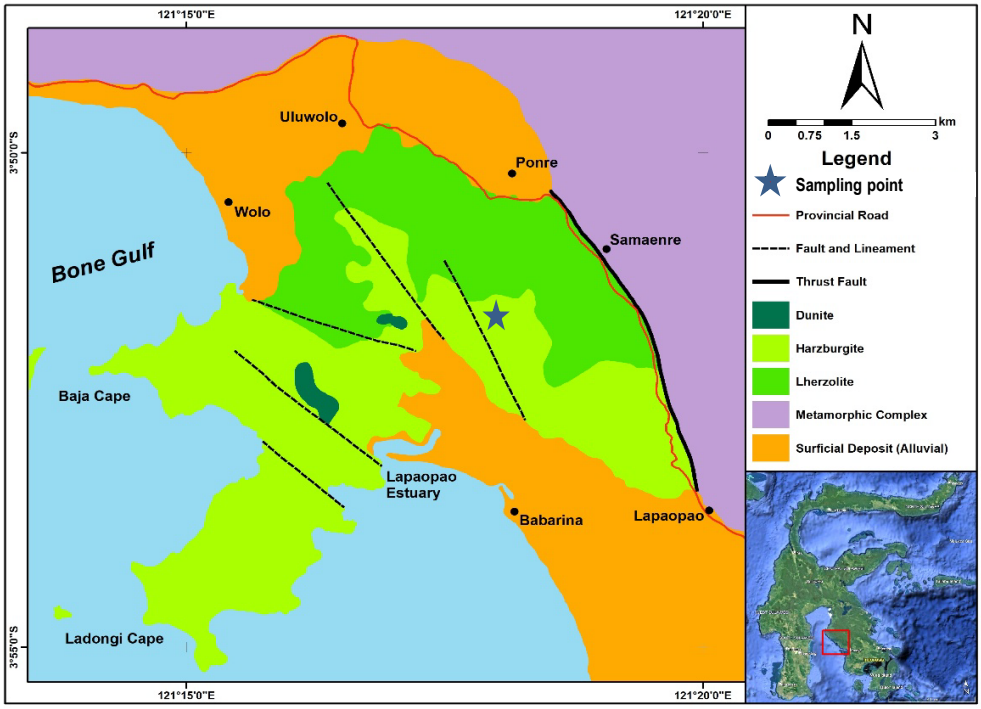


Fig. 1. Geological map of the Wolo mine area and ore sampling location

Rys. 1. Mapa geologiczna obszaru wydobywczego Wolo i lokalizacja pobrania próbek rudy

ground using a ball mill. The powder samples were sieved into four particle size fractions (–80+100, –100+140, –140+200, and –200 mesh). Additionally, charcoal was prepared by heating corncob at 500°C in a closed crucible. The charcoal product was ground using an agate mortar and sieved into the desired particle size. Results of the proximate analysis of corncob charcoal were reported by Sufriadin et al. (2024), and calorific value was measured

Table 1. Proximate analysis and heating value of corncob charcoal used as a reductant

Tabela 1. Analiza składu chemicznego i wartość opałowa węgla drzewnego z kolb kukurydzy stosowanego jako reduktor

| Material | IM (%) | AC (%) | VM (%) | FC (%) | CV (cal/g) |
|---|---|---|---|---|---|
| Corncob Char | 7.17 | 8.62 | 23.98 | 60.22 | 5,901 |

IM – inherent moisture, AC – ash content, VM – volatile matter, FC – fixed carbon, CV – calorific value.
Source: Sufriadin et al. 2024.

using a bomb calorimeter (Table 1). Before reductive roasting and magnetic separation, the laterite ore sample was dried in an oven for 6 hours at 100°C ± 5°C.

### 1.2. Experimental

The reductive-roasting experiment of nickel laterite ore was conducted using a muffle furnace (Yamato FO-310) with a working chamber of 200 × 250 × 150 $mm^3$ and a maximum temperature of 1,200°C. A total of 100 grams of the mixture between a nickel laterite sample and corncob char as a reductant was prepared for every run, with the mass ratio of 9:1. Ore particle sizes taken as variables were –80+100, –100+140, –140+200, and –200 mesh. The closed ceramic crucibles containing 90 g dry ore mixture with 10 g corncob charcoal were then inserted into a muffle furnace. One hour of reduction time and a roasting temperature of 1,000°C were determined as the experimental conditions. Following the completion of the roasting experiment, the crucibles containing roasted ore were taken out of the muffle furnace and put in a desiccator to cool down quickly and minimize re-oxidation. The roasted products were ground to less than 200 mesh before further analyses.

Unroasted laterite ore and roasted products were separated using a low-intensity drum magnetic separator (0.1 T) rotated at 250 rpm. After the separation, magnetic concentrates and tailing were weighted to determine recoveries. All experimental works were conducted at the Mineral Processing Laboratory, Mining Engineering Department, Hasanuddin University.

### 1.3. Analytical Methods

The mineralogical composition of the original ore, magnetic concentrates, and roasted products was analyzed using X-ray diffraction (Shimadzu, Maxima X-7000 diffractometer). The voltage of 40 kV, the electric current of 30 mA, the scanning range of 5° to 70° 2-theta, the scanning steps of 0.02°, and the scanning time of 2°/minute were set as the experimental conditions. The interpretation of minerals or phases present was further performed using the

Impact Match 3 program (trial version). This work was done at the Department of Mining Engineering, Hasanuddin University.

Scanning electron microscopy (SEM, Hitachi High-Technologies SU3500) attached to an EDAX Octane Plus energy-dispersive spectrometry (EDS) was employed to observe the textural features of the ore and to determine the semi-quantitative chemical composition of some spots within the original ore, unroasted magnetic concentrates, and roasted magnetic concentrates. This analysis was conducted at the Faculty of Engineering, Kyushu University.

Determination of the bulk chemical composition of the raw ore, magnetic concentrates, and roasted products was performed using X-ray fluorescence (XRF) spectrometry. For this purpose, about 2 g powder samples with a particle size of less than 75 μm were prepared as press pellet samples before being submitted for analysis. Chemical concentration was measured by a spectrometer (Skyray Instrument, ED-Explorer 5000). This analysis was performed at PT. Anugrah Inti Spectra (AIS) Laboratory and Consultant, Makassar City, Indonesia.

## 2. Results and discussion

### 2.1. Ore characterization

The XRD pattern of nickel laterite ore is shown in Figure 2. It is indicated that the ore sample mainly contains goethite and lizardite, followed by talc, quartz, and smectite. The

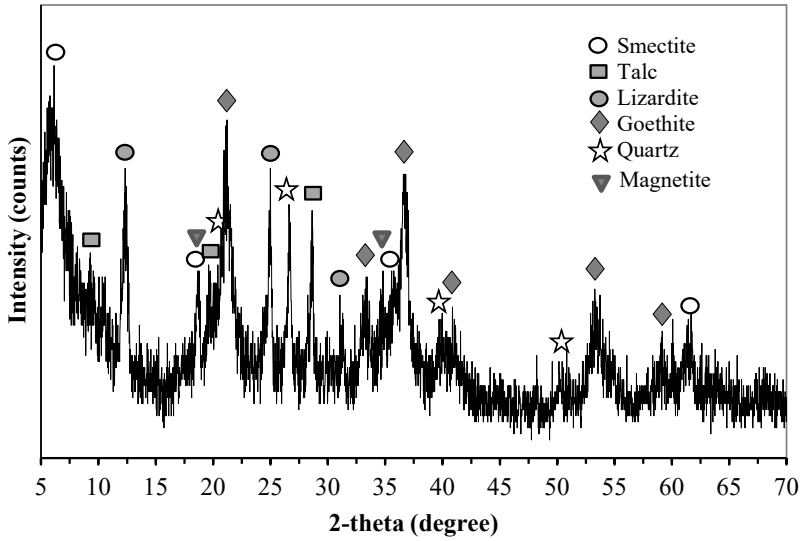


Fig. 2. X-ray diffraction pattern of nickel laterite ore used in this study

Rys. 2. Wzór dyfrakcji rentgenowskiej rudy laterytowej niklu wykorzystanej w niniejszym badaniu

presence of goethite is marked by diffraction peaks with crystal spacings (dhkl) of 14.18Å, 2.69Å, and 2.45Å. The diffraction peaks with d spacing of 9.52Å, 4.75Å, and 3.11Å can be assigned to talc. Reflection intensities with d values of 7.15Å, 3.57Å, and 1.56Å are diagnostic peaks of lizardite, a serpentine group mineral. Quartz is characterized by diffraction peaks with the 2θ angle of 20.74°, 26.64°, 40.04°, and 50.18°, corresponding to the d spacing 4.26Å, 3.34Å, 2.25Å, and 1.82Å. Smectite (likely montmorillonite) is identified with a diagnostic peak at 2θ of 5.88° (15.01Å). In contrast, magnetite is detected with the presence of peaks having $d_{hkl}$ of 4.80Å and 2.53Å, respectively. It is predicted that goethite and lizardite are the principal Ni-bearing phases within the studied ore.

Backscattered electron (BSE) images of representative minerals present in the original ore are given in Figure 3. The ore texture is characterized by anhedral crystals and shows the development of secondary pseudomorphic replacement, forming a bastite texture (Figure 3a) and mesh texture (Figure 3b). The ore also contains minerals characterized by anhedral, elongate, and relatively massive, surrounded by finer particles (Figure 3c).

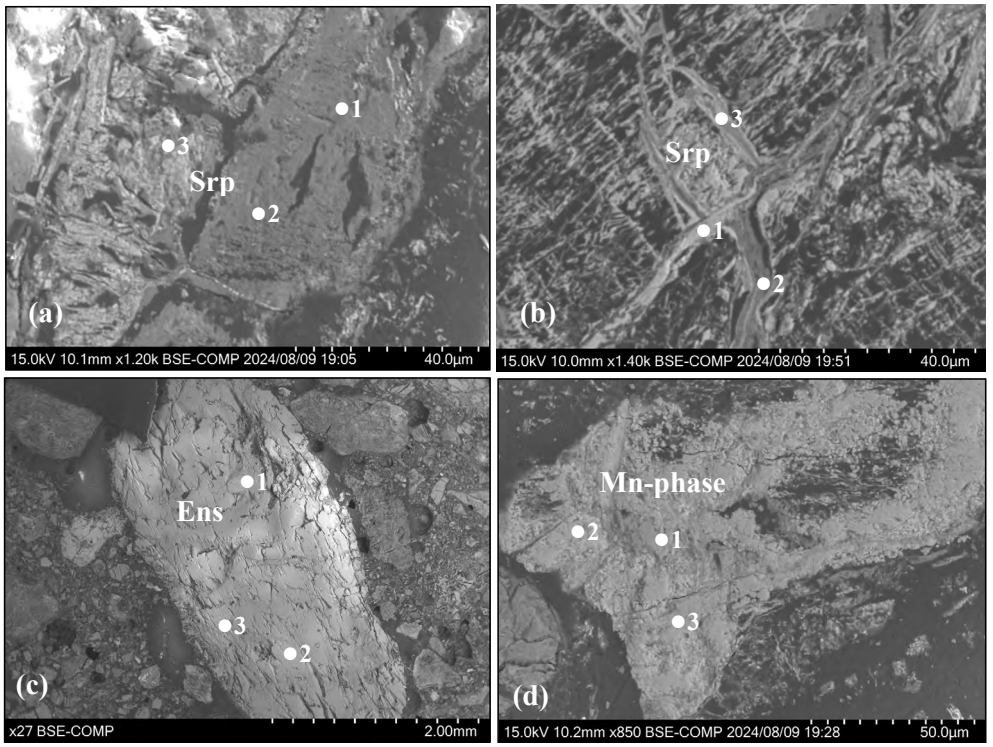


Fig. 3. Backscattered electron (BSE) images of some minerals in the original ore sample. Srp – serpentine, Ens – enstatite

Rys. 3. Obrazy elektronów wstecznie rozproszonych (BSE) niektórych minerałów w oryginalnej próbce rudy. Srp – serpentyn, Ens – enstatyt

The bulk chemical composition of the original Ni-laterite ore sample used in this study is given in Table 2. The Ni concentration of ore shows a relatively higher value, whereas the Fe grade displays a relatively low. Similarly, the content of MgO is also low, but $Al_2O_3$ and $SiO_2$ indicate higher grades. The MnO and CaO contents are also low. The ratio of $SiO_2$/MgO is an extremely high value. The raw ore sample is best categorized as a saprolitic ore type based on the bulk chemical composition and mineralogical nature.

Table 2. Chemical composition of original nickel laterite ore sample (anhydrous basis)

Table 2. Skład chemiczny oryginalnej próbki rudy laterytowej niklu (w stanie bezwodnym)

| Elements/oxides (wt%) | | | | | | | | | $SiO_2$/MgO | Fe/Ni |
|---|---|---|---|---|---|---|---|---|---|---|
| Ni | Fe | $Fe_2O_3$ | $Al_2O_3$ | $SiO_2$ | MgO | MnO | CaO | Co | | |
| 1.90 | 24.97 | 35.71 | 4.87 | 32.58 | 6.84 | 0.24 | 0.59 | 0.05 | 4.76 | 13.14 |

The spot EDX analysis result of the selected minerals in the original ore sample is shown in Table 3. Serpentine is the principal Ni-bearing mineral, having various Ni concentrations ranging between 1.54 and 3.33%. Nickel concentration tends to increase when the Fe grade of serpentine also elevates. In contrast, Mg and Si decreased significantly, indicating that these elements have leached out during the chemical weathering of serpentinized ultramafic rocks. The chemical composition of pyroxene in this ore shows relatively low Fe, and it does not contain Ni. A Mn-rich phase is also found within the ore, characterized by high Mn, Ni, and Co. The average Mn content is 18.28%, whereas Ni and Co have average grades of 11.74% and 1.48%, respectively. The average concentration of Al is also relatively high, with a grade of 9.24%.

## 2.2. Effect of particle sizes on the Fe-Ni grades of the unroasted magnetic fraction

A graph showing the effect of ore particle sizes on the enrichment of Fe and Ni grades of magnetic concentrates is given in Figure 4. It is exhibited that decreasing particle sizes tend to enrich both Ni and Fe. The maximum grade of Ni (2.44%) was achieved at the magnetic concentrate with a grain size of –200 mesh (–75 μm). Similarly, Fe content also significantly increased, with the highest value of 45.47%. Reduction of particle sizes may enhance the liberation degree of Ni-hosted magnetic minerals, leading to the rise of the Fe and Ni grades in the magnetic fraction.

Table 3. Spot EDX analysis of selected minerals in the original laterite ore (the spot positions are shown in Figure 3)

Tabela 3. Analiza punktowa EDX wybranych minerałów w oryginalnej rudzie laterytowej (pozycje punktów pokazano na rys. 3)

| Element (wt%) | Serpentine | | | Fe-rich serpentine | | | Pyroxene | | | Mn-rich phase | | |
|---|---|---|---|---|---|---|---|---|---|---|---|---|
| | a1 | a2 | a3 | b1 | b2 | b3 | c1 | c2 | c3 | d1 | d2 | d3 |
| O | 44.90 | 45.21 | 51.73 | 29.91 | 31.55 | 30.60 | 59.29 | 46.58 | 36.89 | 30.35 | 34.80 | 34.73 |
| Mg | 11.02 | 12.66 | 9.36 | 2.03 | 1.95 | 1.85 | 6.15 | 20.67 | 21.69 | 2.04 | 2.40 | 1.95 |
| Al | 4.05 | 3.78 | 1.86 | 1.54 | 3.56 | 2.42 | 1.48 | 3.00 | 3.40 | 5.98 | 12.85 | 8.89 |
| Si | 23.17 | 24.48 | 17.21 | 11.87 | 16.67 | 10.05 | 31.37 | 26.28 | 30.99 | 9.75 | 2.72 | 9.60 |
| Ca | nd | nd | 0.41 | nd | nd | nd | nd | 1.97 | 2.49 | nd | nd | nd |
| Fe | 14.86 | 12.06 | 17.90 | 51.59 | 42.35 | 49.33 | 1.57 | 1.50 | 4.55 | 30.86 | 4.43 | 13.74 |
| Ni | 1.99 | 1.81 | 1.54 | 2.49 | 2.82 | 3.33 | nd | nd | nd | 9.29 | 13.31 | 12.63 |
| Mn | nd | nd | nd | nd | nd | 1.25 | nd | nd | nd | 9.94 | 28.31 | 16.60 |
| Co | nd | nd | nd | nd | nd | nd | nd | nd | nd | 1.89 | 1.17 | 1.37 |

nd – not detected.

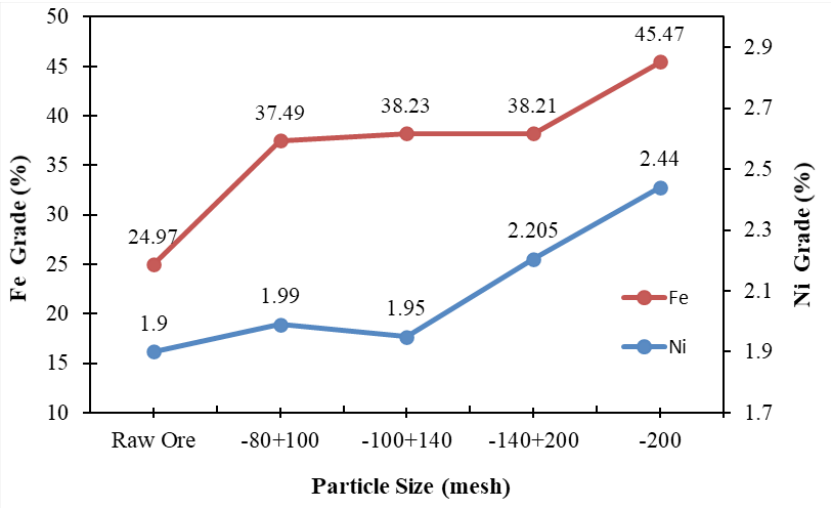


Fig. 4. Graph showing the effect of particle sizes on the Fe-Ni enrichment of unroasted magnetic concentrates

Rys. 4. Wykres przedstawiający wpływ wielkości cząstek na wzbogacenie Fe-Ni w niepalonych koncentratach magnetycznych

SEM analysis of some minerals in a magnetic fraction with the highest Ni content is portrayed in Figure 5, and the representative spot EDX data of selected minerals are shown in Table 4. Goethite has an irregular and acicular texture, with a Ni grade of about 2.54% (Figure 4a). The increase of Fe concentration in goethite is accompanied by the enrichment of Ni, as indicated by chemical data on spots c5 and d1 with the Ni grade of 4.54% and 4.14%, respectively. Magnetite, as the strong magnetic phase, shows various textures from anhedral to euhedral with very bright colors (Figure 5b and 5c). However, magnetite does not contain nickel. One spot (c2), as shown in Figure 5c, indicates a titanomagnetite due to the significant concentration of titanium.

The magnetic fraction also contains silicate phases such as diopside (a pyroxene group). This phase contains a significant concentration of Fe, causing it to become weakly magnetic minerals. However, the diopside does not bear Ni as well. The last Ni-host mineral in the magnetic fraction is lizardite (a serpentine group). The increase in the Ni grade of lizardite is also related to the elevated concentration of Fe in this mineral.

The result of the XRD analysis of unroasted magnetic fractions with different particle sizes is provided in Figure 6. Based on the diffraction patterns, no apparent differences in peak positions between the original ore mineral and magnetic fractions are appreciated. For example, the maximum reflection intensity of lizardite at 12.35° 2θ remains unshifted at both original ore and magnetic fractions. Similarly, the strong reflection intensity peaks of goethite at 21.28° 2θ and 34.35° 2θ both the original ore and corresponding unroasted magnetic fractions are in the same positions.

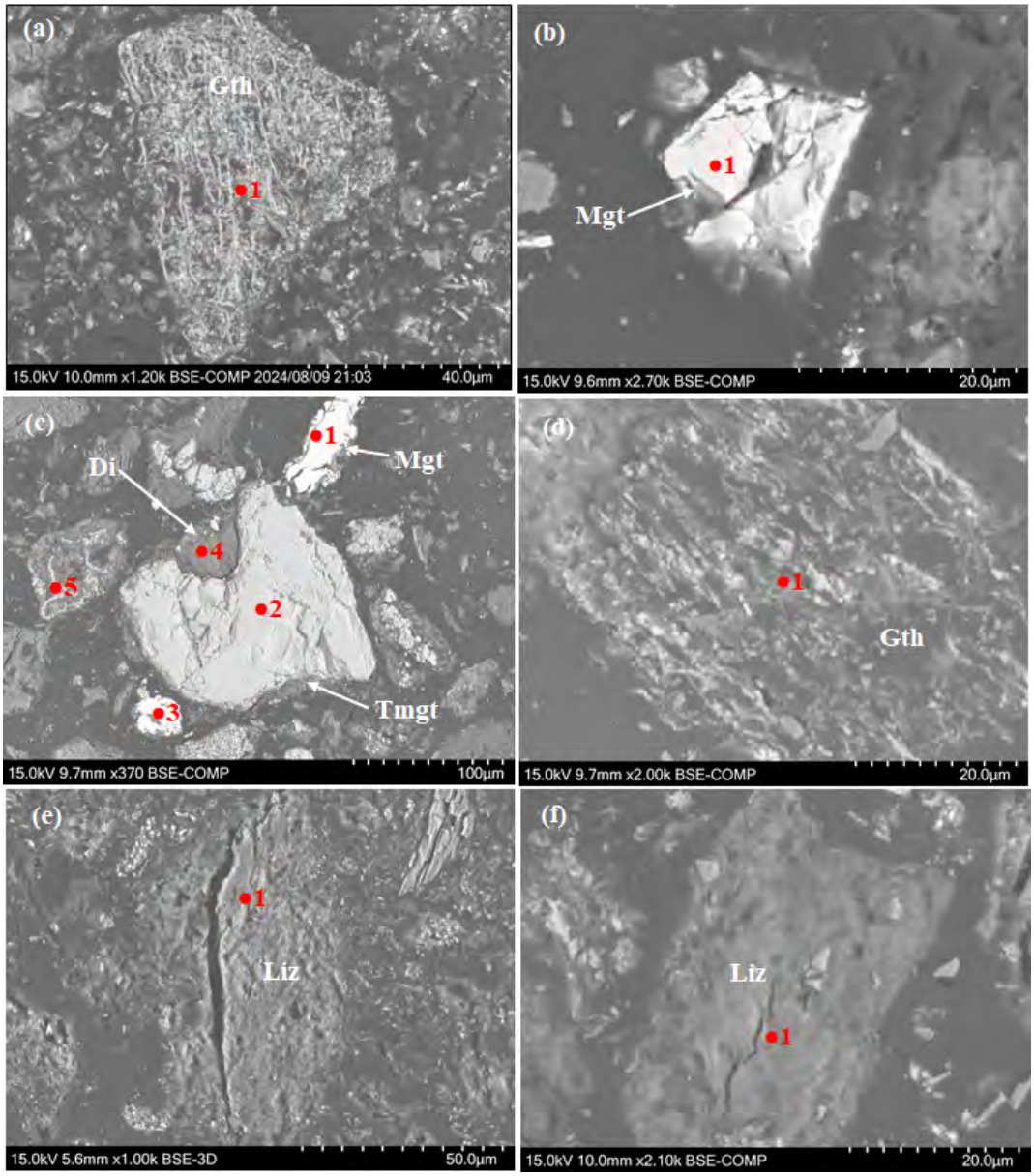


Fig. 5. Backscattered electron (BSE) images of some minerals in unroasted magnetic fraction
Gth – goethite, Mgt – magnetite, Di – diopside, Tmgt – titanomagnetite, Liz – lizardite

Rys. 5. Obrazy elektronów wstecznie rozproszonych (BSE) niektórych minerałów w niepalonej frakcji magnetycznej
Gth – goethyt, Mgt – magnetyt, Di – diopsyd, Tmgt – tytanomagnetyt, Liz – lizardyt

Table 4. Spot EDX analysis of some minerals in unroasted magnetic concentrate

Tabela 4. Analiza EDX niektórych minerałów w niepalonym koncentracie magnetycznym

| Element (wt%) | Gth | Mgt | Mgt | Tmgt | Mgt | Di | Gth | Gth | Liz | Liz |
|---|---|---|---|---|---|---|---|---|---|---|
| | a1 | b1 | c1 | c2 | c3 | c4 | c5 | d1 | e1 | f1 |
| O | 26.32 | 26.40 | 1.14 | 26.00 | 1.32 | 38.10 | 27.73 | 33.13 | 33.86 | 36.13 |
| Mg | nd | nd | nd | nd | nd | 2.29 | 1.07 | 0.72 | 6.21 | 26.61 |
| Al | 3.40 | nd | nd | 2.05 | nd | 19.20 | 3.24 | 1.56 | 2.81 | 0.89 |
| Si | 7.53 | nd | 2.43 | 0.28 | 2.47 | 32.10 | 9.23 | 9.04 | 25.17 | 28.53 |
| Ca | 0.47 | nd | nd | nd | nd | 1.38 | nd | nd | nd | nd |
| Fe | 56.21 | 73.60 | 96.43 | 65.65 | 96.21 | 6.11 | 51.94 | 50.60 | 29.19 | 5.24 |
| Ni | 2.54 | nd | nd | nd | nd | nd | 4.64 | 4.14 | 2.76 | 1.94 |
| Mn | 0.34 | nd | nd | nd | nd | nd | nd | nd | nd | nd |
| Cr | 3.19 | nd | nd | nd | nd | nd | 2.16 | nd | nd | nd |
| Ti | nd | nd | nd | 6.01 | nd | nd | nd | nd | nd | nd |

nd – not detected, Gth – Goethite, Mgt – Magnetite, Tmgt – Titanomagnetite, Di – Diopside, Liz – Lizardite.

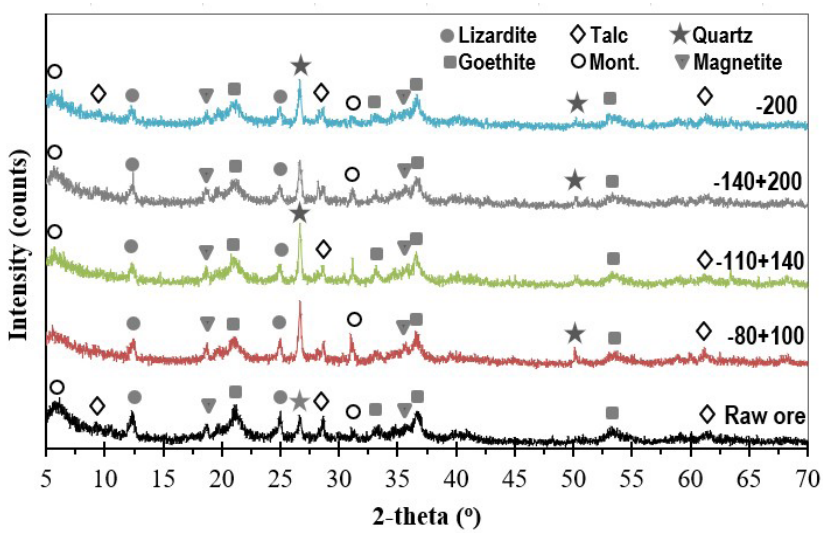


Fig. 6. X-ray diffraction patterns of the raw ore and unroasted magnetic concentrates with different particle sizes

Rys. 6. Wzory dyfrakcji rentgenowskiej surowej rudy i niepalonych koncentratów magnetycznych o różnych rozmiarach cząstek

### 2.3. The effect of particle sizes on Fe-Ni grade of roasted magnetic fractions

A comparison between the Fe-Ni grade of laterite raw ore and its associated roasted magnetic fractions with various grain sizes is depicted in Figure 7. It is revealed that Ni concentration increased to 2.14% at –80+100 mesh sizes as compared to 1.90% in the raw ore. The Ni grade slightly decreases with a decrease in particle size down to –100+140 mesh. Reduction of particle sizes to –140+200 mesh results in the maximum enrichment of Ni up to 2.17%. Further particle size reduction to –200 mesh shows a slight decrease in Ni grade, becoming 2.12%. However, it generally indicates that the reduction in grain size is linearly correlated with the increase in Ni content.

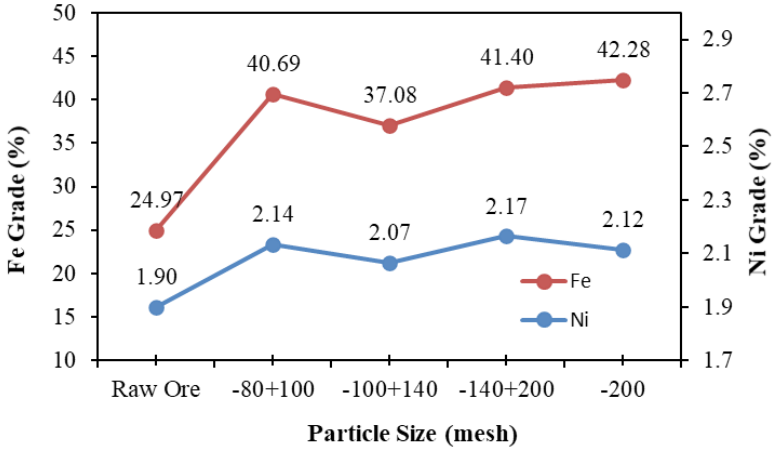


Fig. 7. Graph showing the effect of particle size on the Ni-Fe grade of roasted magnetic fractions

Rys. 7. Wykres przedstawiający wpływ wielkości cząstek na zawartość niklu i żelaza we frakcjach magnetycznych po prażeniu

The effect of particle sizes on the Fe enrichment patterns of roasted magnetic fractions exhibits similarity with Ni. The Fe concentration increases at –80+100 mesh (40.69%) from 24.97% in the raw ore. However, particle size reduction down to –100+140 mesh is accompanied by a decline in the Fe grade to 37.08%. Further reduction of particle sizes at –140+200 and –200 mesh shows enrichment in Fe with the values of 41.40% and 42.28%, respectively.

Backscattered electron images of roasted magnetic fractions are provided in Figure 8, whereas spots' EDX data of selected minerals are shown in Table 5. It is revealed that some minerals were formed during roasting, such as silicates (enstatite and olivine), Ti-Fe-rich spinel, Ni-spinel (trevorite), and Fe-Ni alloys. Enstatite is characterized by anhedral texture and missive. It contains higher Fe but lower Mg with a small quantity of Cr (Figure 8a).

Table 5. EDX analysis of some points on minerals in roasted magnetic fractions

Table 5. Analiza EDX niektórych punktów na minerałach w prażonych frakcjach magnetycznych

| Element (wt%) | Ens | | Ti-Spl | | FeNi | | Qz | Tr | FeNi | Ol |
|---|---|---|---|---|---|---|---|---|---|---|
| | a1 | a2 | b1 | b2 | d1 | e1 | e2 | e3 | f1 | f2 |
| O | 45.96 | 47.79 | 46.15 | 45.32 | nd | nd | 66.79 | 47.16 | nd | 56.31 |
| Mg | 11.60 | 15.11 | 5.06 | 5.67 | nd | nd | nd | 3.80 | nd | 13.80 |
| Al | 0.83 | 1.21 | 5.05 | 5.22 | nd | nd | nd | 5.15 | nd | 1.22 |
| Si | 30.05 | 31.05 | 0.77 | 1.69 | nd | nd | 33.21 | 8.59 | nd | 19.85 |
| Ca | nd | nd | nd | nd | nd | nd | nd | nd | nd | nd |
| Fe | 11.57 | 4.83 | 36.61 | 35.61 | 79.70 | 92.67 | nd | 30.92 | 78.75 | 6.96 |
| Ni | nd | nd | nd | nd | 20.30 | 7.68 | nd | 4.38 | 21.25 | nd |
| Mn | nd | nd | nd | nd | nd | nd | nd | nd | nd | 1.86 |
| Cr | 3.19 | nd | nd | nd | nd | nd | nd | nd | nd | nd |
| Ti | nd | nd | 6.36 | 6.48 | nd | nd | nd | nd | nd | nd |

nd – not detected, Ens – enstatite, Ti-Spl – Ti-spinel, Qz – quartz, Tr – trevorite, Ol – olivine.

Spinel was detected in the roasted product, which showed irregular texture and Fe-Ti-rich. Another spinel phase that might be formed was a Ni-rich spinel or trevorite (Figure 8e and Table 5).

The metallization of Fe-Ni alloys is the main target of this study. As shown in Figure 8c–f, the growth of Fe-Ni alloy particles is characterized by a rounded to subrounded texture with particle sizes ranging between ~0.5 µm and 20 µm. They are surrounded by silicate phases such as quartz, enstatite, and olivine (dark color). The EDX analysis results of Fe-Ni alloys (see Table 5) exhibit Ni content of approximately 20–21% and 8%, respectively. These compositions are corresponding to tetrataenite and kamachite, respectively.

## 2.4 Recoveries of Fe-Ni

Recovery in mineral processing is a parameter that describes the amount of valuable mineral or metal successfully extracted from raw ore during the beneficiation process. However, the success of a mineral processing operation depends not only on the recovery

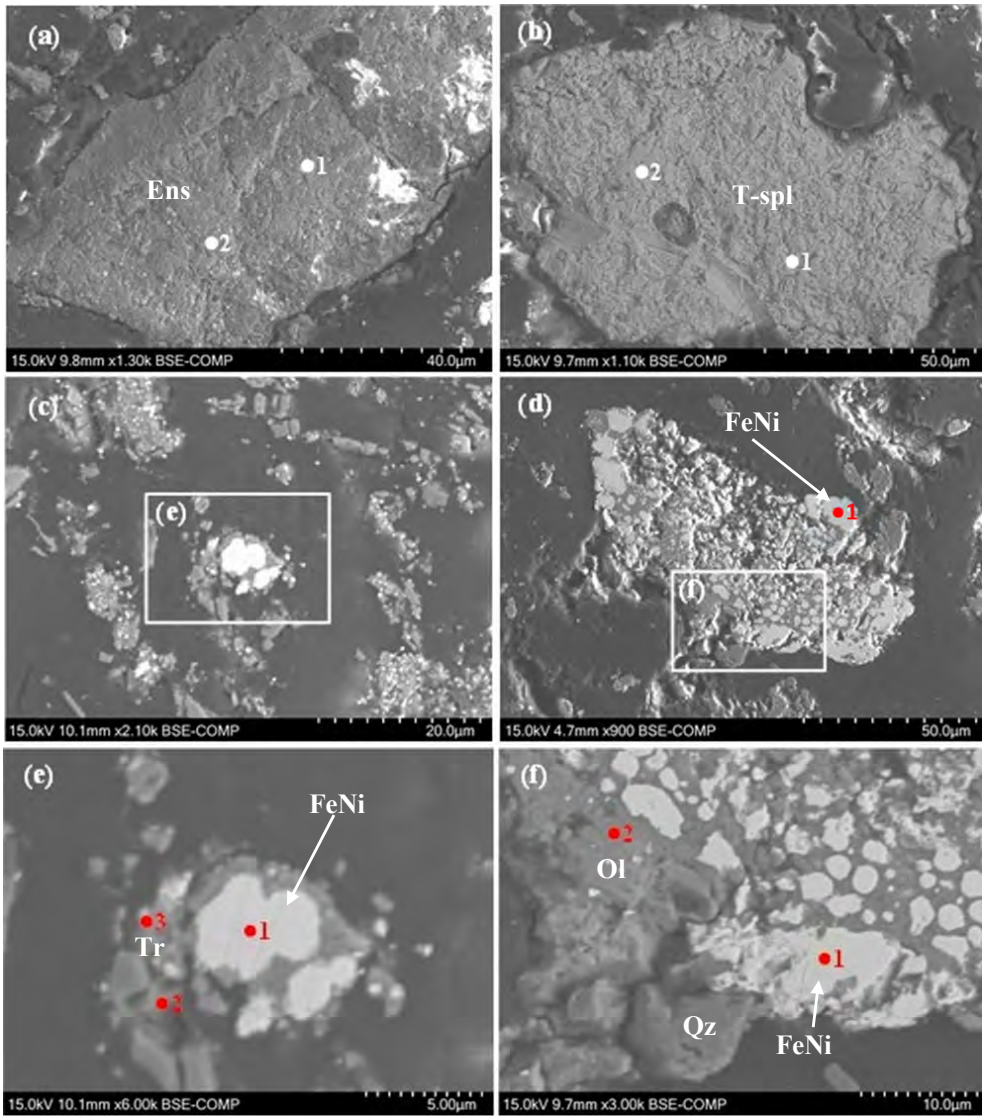


Fig. 8. Backscattered electron (BSE) images show some minerals in roasted magnetic concentrates (a–b) silicate phases, (c–d) Fe-Ni alloys, and (e–f) enlargement image portions at images c and d, respectively Ens – enstatite, Tspl – titanium spinel, Qz – quartz, Ol – olivine

Rys. 8. Obrazy elektronów wstecznie rozproszonych (BSE) pokazują niektóre minerały w prażonych koncentratach magnetycznych (a–b) fazy krzemianowe, (c–d) stopy Fe-Ni oraz (e–f) powiększone fragmenty obrazów c i d Ens – enstatyt, Tspl – spinel tytanowy, Qz – kwarc, Ol – oliwin

rate achieved but also on the ratio of concentration and the grade of product obtained. Estimation of metal recoveries in the beneficiation products can be determined by using the following equation (Wills and Finch 2016):

$$R = [(C \cdot c)/(F \cdot f)] \cdot 100\% \quad (1)$$

- R – recovery rate (%),
- C – weight of concentrate,
- c – grade of metal in concentrate,
- F – weight of feed,
- f – grade of metal in feed.

Results of Ni and Fe recoveries showing the effect of particle size in both unroasted and roasted magnetic concentrate are displayed in Figure 9. It is expressed that the effect of particle sizes of unroasted and roasted magnetic fractions for the Ni recovery fluctuates (Figure 9a). However, the fluctuation pattern shows an inverse relation. A similar case can be seen when Fe recovery is compared between unroasted and roasted magnetic fractions (Figure 9b). The maximum Ni recovery of 81.13% was achieved at the roasted magnetic fraction with the particle size of –140+200 mesh. In contrast, only 15.95% of Ni could be recovered from the unroasted magnetic fraction at the particle size of –200 mesh. Similarly, the maximum Fe recovery of about 99.49% could be obtained from the roasted magnetic fraction at the particle size of –140+200 mesh. In comparison, only 26.26% of Fe could be recovered from unroasted magnetic fractions.

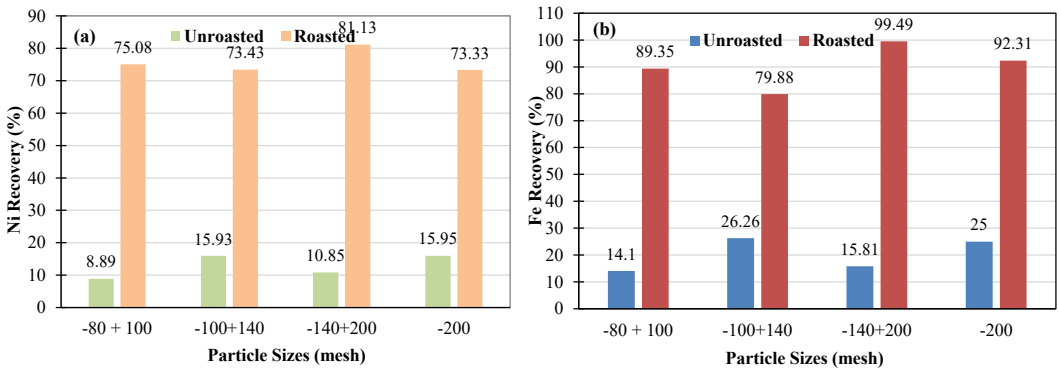


Fig. 9. Recovery of Ni (a) and Fe (b) through magnetic separation at various particle sizes, both unroasted and roasted laterite ore

Rys. 9. Odzysk niklu (a) i żelaza (b) poprzez separację magnetyczną przy różnych rozmiarach cząstek, zarówno w przypadku niepalonej, jak i palonej rudy laterytowej

### 2.5. Mechanism of reductive roasting and phase transformation

The X-ray diffraction patterns of the original ore and subsequent magnetic products resulting from reductive roasting using corncob charcoal reductant are shown in Figure 10. It is exhibited that particle sizes induce no appreciable phase changes. As the dominant mineral, the Fe-rich lizardite, and possibly other silicate phases such as talc and montmorillonite contained in the ore, have first undergone de-hydroxylation during roasting. Similarly, goethite begins to dehydroxylate at around 200°C and changes into proto-hematite. Further, increased reduction temperature up to 1,000°C, has led to the transformation of lizardite into enstatite or the form of oxide phases, whereas goethite transformed into hematite.

The thermal breakdown of the principal Ni-bearing phases (lizardite and goethite) might follow the chemical reactions (Crundwell et al. 2012):

$$(Fe, Ni, Mg)_3Si_2O_5(OH)_{4(s)} \rightarrow FeO_{(s)} + NiO_{(s)} + MgO_{(s)} + SiO_{2(s)} + H_2O_{(g)} \quad (2)$$

$$2FeOOH_{(s)} \rightarrow Fe_2O_{3(s)} + H_2O_{(g)} \quad (3)$$

With the presence of carbon supplied by corncob charcoal, the iron and nickel oxide phases were then reduced into metallic forms. The chemical reactions, along with standard free energy during solid state reduction of Fe and Ni, are shown in Table 6 (Marzoughi and Pickles 2024; Wang et al. 2024):

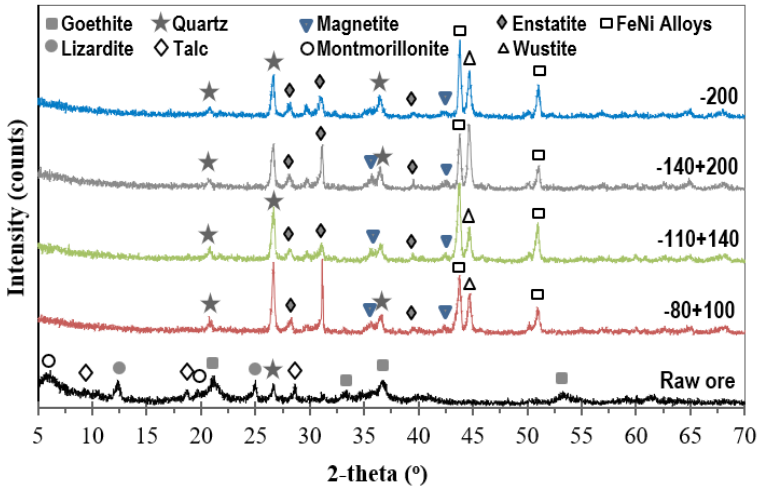


Fig. 10. X-ray diffraction patterns of raw laterite ore and roasted magnetic concentrates reduced at 1000°C, 1 hour retention time and using 10% dosage of corncob charcoal reductant

Rys. 10. Wzory dyfrakcji rentgenowskiej surowej rudy laterytowej i prażonych koncentratów magnetycznych zredukowane w temperaturze 1000°C, przy czasie retencji 1 godzina i przy użyciu 10-procentowej dawki reduktora z węgla drzewnego z kolb kukurydzy

The growth of Fe-Ni particles, as depicted in Figure 8c–f, shows finely disseminated grains, and they are surrounded by silicate phases such as enstatite and high quartz. A relatively low grade of Ni in the roasted magnetic fraction compared to that of the unroasted magnetic fractions might partly be due to the presence of non-magnetic, barren silicate phases that hamper further magnetic separation of Fe-Ni alloys. The very fine grain sizes of Fe-Ni alloys are likely another factor that hinders their concentration.

A comparison of reductive roasting using various reductants between this paper and some previously reported studies of Ni-laterite ores from Indonesia (Sufriadin et al. 2024; Guo et al. 2021; Suharno et al. 2021; Shofi et al. 2019; Mayangsari et al. 2018) is provided in Table 7. It is revealed that Ni enrichment during reductive roasting is not only affected by

Table 6. Chemical reactions and $\Delta G_T^o - T$ of iron and nickel oxides reduction

Tabela 6. Reakcje chemiczne i $\Delta G_T^o - T$ redukcji tlenków żelaza i niklu

| | Chemical Equation | $\Delta G_T^o - T$ (J/mol) |
|---|---|---|
| (a) | $3Fe_2O_{3(s)} + C_{(s)} \rightarrow 2Fe_3O_{4(s)} + CO_{(g)}$ | 237,700 – 222.0 T |
| (b) | $3Fe_2O_{3(s)} + CO_{(g)} \rightarrow 2Fe_3O_{4(s)} + CO_{2(g)}$ | –52,130 – 41.0 T |
| (c) | $Fe_3O_{4(s)} + CO_{(g)} \rightarrow 3FeO_{(s)} + CO_{2(g)}$ | 35,380 – 40.2 T |
| (d) | $Fe_3O_{4(s)} + C_{(s)} \rightarrow 3FeO_{(s)} + CO_{(g)}$ | 262,350 – 179.7 T |
| (e) | $FeO_{(s)} + CO_{(g)} \rightarrow Fe_{(s)} + CO_{2(g)}$ | –10,556 – 17.69 T |
| (f) | $C_{(s)} + CO_{(g)} \rightarrow CO_{2(g)}$ | 170,700 – 174.5 T |
| (g) | $NiO_{(s)} + C_{(s)} \rightarrow Ni_{(s)} + CO_{(g)}$ | 122,207 – 172.8 T |
| (h) | $NiO_{(s)} + CO_{(g)} \rightarrow Ni_{(s)} + CO_{2(g)}$ | –37,600 – 11.8 T |

Table 7. Comparison of reductive roasting using various reductants of Ni-laterite ores from Indonesia

Tabela 7. Porównanie redukcyjnego prażenia przy użyciu różnych reduktorów rud laterytowych niklu z Indonezji

| Ore type | Location | Ni (%) | Fe (%) | Reductant | Reduction temp/time | Ni grade/rec. | Fe grade/rec. | Source |
|---|---|---|---|---|---|---|---|---|
| Saprolite | Wolo, Sulawesi | 1.90 | 24.97 | Corncob charcoal | 1,000°C/1 h | 2.17/83.13 | 41.8/99.5 | This Study |
| Saprolite | Obi Island | 1.53 | 18.84 | Corncob charcoal | 1,000°C/1 h | 1.88/84.28 | 14.2/51.8 | Sufriadin et.al. 2024 |
| Limonite | Indonesia | 1.16 | 46.55 | Straw charcoal | 1,250°C/80 min. | 1.81/97.21 | 81.4/98.8 | Guo et al. 2021 |
| Limonite | Sulawesi | 1.40 | 50.50 | Palm kernel shell char | 1,150°C/1 h | 4.60/73.20 | 81.9/35.0 | Shofi et al. 2019 |
| Limonite | Sulawesi | 1.40 | 50.50 | Anthracite | 1,050°C/1 h | 2.00/85.80 | 61.5/74.7 | Suharno et al. 2021 |
| Limonite | Halmahera | 1.29 | 27.02 | Coal | 1,100°C/1 h | 4.34/50.38 | 57.5/37.6 | Mayangsari et al. 2018 |

the dosages of reductants but also by other parameters such as reduction temperature and roasting duration. It is not clear whether the types of reductants might affect the Ni grade of roasted products.

To maximize the Ni grade and limit Fe reduction, it is suggested that the roasting temperature above 1,000°C be increased, and additives such as $NaSO_4$ or $CaSO_4$ should be considered to enhance Fe-Ni particle growth and restrict Fe reduction.

## Conclusions

Magnetic separation was employed for a nickel laterite sample to elucidate the effect of ore particle size variations on the enrichment of Fe-Ni in unroasted ore and roasted laterite ore using corncob charcoal reductant. The major conclusions of this study can be summarized as follows:

1. The mineralogical analysis of the ore sample shows that lizardite and goethite are the main Ni-bearing minerals, characterized by higher Fe and lower MgO. The bulk Ni composition of the sample is 1.90%.
2. Results of magnetic beneficiation of the ore sample indicate that decreasing particle sizes tend to enrich Fe-Ni grades both in unroasted and roasted concentrates. This might be due to the increased liberation of magnetic minerals that bear Ni. However, Fe-Ni recoveries of unroasted concentrates are much lower than those of roasted products.
3. Reductive roasting of laterite ore using corncob charcoal as a reductant has led to a strong increase in the magnetic properties of the concentrate and the development of Fe-Ni particle growth. However, silicate phases also formed that envelop Fe-Ni alloys, leading to difficulty in maximizing Ni grade in concentrates.

*The Authors have no conflict of interest to declare.*

*The authors would like to acknowledge the Head of Institute for Research and Community Service (LP2M), Hasanuddin University, for financial support under the scheme of Fundamental Research Collaboration (FRC), contract No. 00309/UN4.22/PT.01.03/2024. Thanks to Dr. Suharto (PT. CNI Company) for supplying the Ni-laterite samples.*

## REFERENCES

Butt, C.R.M., and Cluzel, D. 2013. Nickel Laterite Ore Deposits: Weathered Serpentinites. *Elements* 9, pp. 123–128, DOI: 10.2113/gselements.9.2.123.

Chen et al. 2016 – Chen, G.J., Shiau, J.S., Liu, S.H. and Hwang, W.S. 2016. Optimal Combination of Calcination and Reduction Conditions as well as $Na_2SO_4$ Additive for Carbothermic Reduction of Limonite Ore. *Materials Transactions* 57(9), pp. 1560–1566, DOI: 10.2320/matertrans.M2016072.

Crundwell et al. 2011 – Crundwell, F.K., Moats, M.S., Ramachandran, V., Robinson, T.G. and Devenport, W.G. 2011. *Extractive Metallurgy of Nickel, Cobalt, and Platinum-Group Metals.* Amsterdam: Elsevier.

Elliot et al. 2016 – Elliott, R., Pickles, C.A. and Forster, J. 2016. Thermodynamics of the Reduction Roasting of Nickeliferous Laterite Ores. *Journal of Minerals and Materials Characterization and Engineering* 4, pp. 320–346, DOI: 10.4236/jmmce.2016.46028.

Elliot et al. 2017 – Elliot, R., Pickles, C.A. and Peacey, J. 2017. Ferronickel particle formation during the carbothermic reduction of a limonitic laterite ore. *Minerals Engineering* 100, pp. 166–176, DOI: 10.1016/j.mineng.2016.10.020.

Fan et al. 2024 – Fan, Q., Yuan, S., Wen, J. and He, J. 2024. Review on comprehensive utilization of nickel laterite ore. *Minerals Engineering* 218, DOI: 10.1016/j.mineng.2024.109044.

Forster et al. 2016 – Forster, J.A., Pickles, C.A. and Elliott, R. 2016. Microwave carbothermic reduction roasting of a low-grade nickeliferous silicate laterite ore. *Minerals Engineering* 88, pp. 18–27, DOI: 10.1016/j.mineng.2015.09.005.

Guo et al. 2021 – Guo, X.S., Li, Z.Y., Han, J.C., Yang, D. and Sun, T.C. 2021. Study of straw charcoal as a reductant in co-reduction roasting of laterite ore and red mud to prepare powdered ferronickel. *Mining, Metallurgy and Exploration* 38, pp. 2217–2228, DOI: 10.1007/s42461-021-00466-z.

Kim et al. 2010 – Kim, J., Dodbiba, G., Tanno, H., Okaya, K., Matsuo, S. and Fujita, T. 2010. Calcinations of low-grade laterite for concentration of Ni by Magnetic Separation. *Minerals Engineering* 23(4), pp. 282–288, DOI: 10.1016/j.mineng.2010.01.005.

Marzoughi, O. and Pickles, C.A. 2024. Solid state reduction and magnetic separation of nickeliferous laterite ores: Review and analysis. *Journal of Industrial and Engineering Chemistry* 140, DOI: 10.1016/j.jiec.2024.05.056.

Mayangsari et al. 2018 – Mayangsari, W., Prasetyo, A.B. and Prasetiyo, P. 2018. Upgrading nickel content of limonite nickel ore through pelletization, selective reduction, and magnetic separation. Proceedings of the *3rd International Conference on Materials and Metallurgical Engineering and Technology (Icommet 2017)*: Advancing Innovation in Materials Science, Technology and Applications for Sustainable Future, Surabaya, Indonesia, DOI: 10.1063/1.5030243.

Nickel Institute –*About Nickel*. [Online:] https://nickelinstitute.org/about-nickel/ [Accessed: 2023-08-17].

Nurjaman et al. 2021 – Nurjaman, F., Astuti, W., Bahfie, F. and Suharno, B. 2021. Study of selective reduction in lateritic nickel ore: Saprolite versus limonite. *Material Today* 44, pp. 1488–1494, DOI: 10.1016/j.matpr.2020.11.687.

Shofi et al. 2019 – Shofi, A., Rahmahwati, A., Nurjaman, F. and Suharno, B. 2019. Effect of reduction temperature and sodium-based additives on nickel upgrading process of laterites ores. *IOP Conference Series: Materials Science and Engineering* 541, DOI: 10.1088/1757899x/541/1/012002.

Subagja et al. 2016 – Subagja, R., Prasetyo, A.B. and Sari, M. W. 2016. Upgrading of Ni content in limonitic laterite ore by pelletizing, reduction roasting, and magnetic separation of the mixed ore, coal, and sodium sulfate. *Metalurgi* 31(2), DOI: 10.14203/metalurgi.v31i2.156.

Sufriadin et al. 2024 – Sufriadin, A.R., Fauth, S., Tindoilo, P.D., Nur, I., Purwanto, Irfan, U.R., Basir, D.N. and Otake, T. 2024. Thermal Beneficiation of a Nickel Laterite Ore from the Obi Island of North Maluku, Indonesia Using Corncob Char as Reductant. *Advances in Science and Technology* 141, pp. 95–102, DOI: 10.4028/p-05hkM3.

Suharno et al. 2021 – Suharno, B., Nurjaman, F., Ramadini, C. and Shofi, A. 2021. Additives in selective reduction of lateritic nickel ores: Sodium sulfate, sodium carbonate, and sodium chloride. *Mining, Metallurgy and Exploration* 38, pp. 2145–2159, DOI: 10.1007/s42461-021-00456-1.

Wang et al. 2024 – Wang, W., Hu, S., Wang, S., Liu, H., Yu, D., Liu, L., W.H. and Wang, K. 2024. Preparation of Nickel–Iron Concentrate from Low-Grade Laterite Nickel Ore by Solid-State Metalized Reduction and Magnetic Separation. *Minerals* 14, DOI: 10.3390/min14090926.

Wills et al. 2016 – Wills, B.A. and Finch, J.A. 2016. *Mineral Processing Technology: An Introduction to the Practical Aspects of Ore Treatment and Mineral Recovery.* New York: Pergamon Press, 550 pp.

Zappala et al. 2024 – Zappala, L., McDonald, R. and Pawnceby, M.I. 2024. Nickel Laterite Beneficiation and Potential for Upgrading Using High-Temperature Methods: A Review. *Mineral Processing and Extractive Metallurgy Review* 45(7), pp. 767–789, DOI: 10.1080/08827508.2023.2265533.

## BENEFICIATION OF A LATERITIC NICKEL ORE FROM THE WOLO MINE AREA, SOUTHEAST SULAWESI, INDONESIA, THROUGH REDUCTIVE ROASTING AND MAGNETIC SEPARATION

Keywords

laterite ore, reductive roasting, magnetic separation, grain size, nickel grade

Abstract

Treatment of a nickel laterite ore sample from the Wolo mine area of Southeast Sulawesi, Indonesia, has been performed at a low-intensity magnetic separator before and after roasting the ore using corncob charcoal as a reductant. This paper aims to analyze the effect of particle sizes on Fe-Ni enrichment and recoveries of both unroasted and roasted magnetic fractions. Mineralogical analysis of the ore sample, unroasted and roasted products, was carried out using X-ray diffraction (XRD) and scanning electron microscope-energy dispersive spectrometry (SEM-EDX) techniques, respectively, while the chemical composition of the ore sample, unroasted, and roasted magnetic products was determined employing X-ray fluorescence (XRF) spectrometry. Samples with different particle sizes (–80+100, –100+140, –140+200, and –200) mesh were magnetically separated before and after being roasted at 1,000°C for 1 hour with 10% reductant. The SEM-EDX results showed that Ni is mainly hosted in lizardite and goethite. The beneficiation result reveals that the smaller particle size exhibits a higher Ni grade than the larger one. This is shown in the unroasted products, where the maximum grade occurs in the –200 mesh fraction, increasing the Ni grade from 1.9% in raw ore to 2.44% in unroasted magnetic products. Meanwhile, the roasted products have the maximum Ni grade in the –140+200 mesh fraction, increasing the Ni grade from 1.9% in raw ore to 2.17% in roasted magnetic fraction. However, the Ni recovery of unroasted concentrates is much lower (10.85%) than that of roasted products (81.13%).

## WZBOGACANIE RUDY NIKLU LATERYTOWEGO Z OBSZARU WYDOBYWCZEGO WOLO W POŁUDNIOWO-WSCHODNIEJ CZĘŚCI WYSPY SULAWESI W INDONEZJI POPRZEZ PRAŻENIE REDUKCYJNE I SEPARACJĘ MAGNETYCZNĄ

Słowa kluczowe

ruda laterytowa, prażenie redukcyjne, separacja magnetyczna, wielkość ziarna, zawartość niklu

Streszczenie

Przetwarzanie próbki rudy laterytowej niklu z obszaru wydobywczego Wolo w południowo-wschodniej części wyspy Sulawesi w Indonezji przeprowadzono przy użyciu separatora magnetycznego o niskiej intensywności przed prażeniem rudy z wykorzystaniem węgla drzewnego z kolb kukurydzy jako reduktora i po tym procesie. Niniejszy artykuł ma na celu analizę wpływu wielkości cząstek na wzbogacenie Fe-Ni i odzysk zarówno nieprażonych, jak i prażonych frakcji magnetycznych. Analizę mineralogiczną próbki rudy, produktów niepalonych i palonych przeprowadzono

odpowiednio za pomocą dyfrakcji rentgenowskiej (XRD) i skaningowego mikroskopu elektronowego ze spektrometrią dyspersji energii (SEM-EDX), natomiast skład chemiczny próbki rudy, produktów magnetycznych niepalonych i palonych określono za pomocą spektrometrii fluorescencji rentgenowskiej (XRF). Próbki o różnych rozmiarach cząstek (–80+100, –100+140, –140+200 i –200) zostały poddane separacji magnetycznej przed prażeniem w temperaturze 1000°C przez 1 godzinę z dodatkiem 10% reduktora i po tym procesie. Wyniki SEM-EDX wykazały, że Ni występuje głównie w lizardicie i goethicie. Wyniki wzbogacania pokazują, że mniejsze cząstki charakteryzują się wyższą zawartością niklu niż większe. Widać to w produktach niepalonych, gdzie maksymalna zawartość występuje w frakcji –200 mesh, zwiększając zawartość niklu z 1,9% w surowej rudzie do 2,44% w niepalonych produktach magnetycznych. Tymczasem produkty prażone charakteryzują się maksymalną zawartością niklu w frakcji o uziarnieniu –140+200 mesh, co oznacza wzrost zawartości niklu z 1,9% w rudzie surowej do 2,17% w prażonej frakcji magnetycznej. Jednak wydajność odzysku niklu z nieprażonych koncentratów jest znacznie niższa (10,85%) niż w przypadku produktów prażonych (81,13%).